sciendo

Environmental & Socio-economic Studies

DOI: 10.2478/environ-2024-0007

Environ. Socio.-econ. Stud., **2024, 12, 1: 69-80**

Original article

Land use and land cover change in East Java from 2015 to 2021: Use optical imagery and Google Earth engine

Marga Mandala[1], Indarto Indarto[1]*, Nova Nevila Rodhi[2], Akhmad Andi Saputra[3], Farid Lukman Hakim[1]

[1]University of Jember, Faculty of Agricultural, Department of Soil Science, Jl. Kalimantan No. 37, Kampus Tegalboto, Jember, 68121, East Java, Indonesia
[2]University of Jember, Faculty of Agricultural Technology, Department of Agricultural Engineering, Jl. Kalimantan No. 37, Kampus Tegalboto, Jember, 68121, Indonesia
[2]University of Bojonegoro, Faculty of Sains and Engineering, Department of Civil Engineering, Jl. Lettu Suyitno No 2 Kalirejo, Bojonegoro, 62119, East Java, Indonesia
[3]University of Gresik, Faculty of Engineering, Department of Civil Engineering, Jl. Arif Rahman Hakim Gresik No.2B, Kramatandap, Gapurosukolilo, Gresik, 61111, East Java, Indonesia
*E–mail address (*corresponding author): indarto.ftp@unej.ac.id*
ORCID iD: Marga Mandala: https://orcid.org/0000-0002-0851-0027; Indarto Indarto: https://orcid.org/0000-0001-6319-6731; Nova Nevila Rodhi: https://orcid.org/0000-0003-3185-1310; Akhmad Andi Saputra: https://orcid.org/0000-0002-8055-6492; Farid Lukman Hakim: https://orcid.org/0000-0002-9669-7767

ABSTRACT

This study analysed the changes in land use and land cover (LULC) in East Java Province by comparing two LULC maps interpreted from optical imagery. The images captured from 2015 to 2017 were selected to represent the initial LULC maps. Then, the images collected from 2020 to 2021 were considered the recent LULC maps. The input imagery was prepared using the Google Earth engine (GEE). The Random Forest algorithm was used for classification. In this study, eight significant LULC classes were categorised, i.e., built-up area (BU), heterogeneous-agricultural land (HAL), bare soil (BS), paddy field (PF), open water (OW), vegetation (VG), shrubland (SH), and wetland (WL). Next, the training samples were interpreted from Google Earth Pro. Then, the GEE satellite base map and the ground control points (GCPs) were collected. The collected GCPs were split into 70% training and 30% validation data. The results showed that significant LULC Change was more marked in the most urbanised areas (in and around the big cities), followed by LULC change in and around medium towns and rural areas. Four classes experienced an area increase, i.e., BU (+30.23%), HAL (+30.77%), BS (+24.52%), and PF (+14.36%). As a consequence, the other four classes compensated for the increase, i.e., OW (-32.79%), VG (-25.72%), SH (-6.59%), and WL (-25.53%). Regional development from 2015 to 2021 has increased built-up areas. Conversely, the development has reduced OW, VG, SH, and WL. The LULC changes have significantly changed the natural landscape to a human-dominated one.

KEY WORDS: LULC change, random forest algorithm, Sentinel, East Java

ARTICLE HISTORY: received 14 August 2023; received in revised form 1 February 2024; accepted 6 February 2024

1. Introduction

Land use and land cover (LULC) mapping is a critical subject explored by many researchers (Fonji & Taff, 2014; Gashu & Gebre-Egziabher, 2018; Hassan et al., 2016; Hu et al., 2019; Shih et al., 2021). The information of LULC change will beneficial for monitoring and even modelling the trend of changes in LULC (Aksoy & Kaptan, 2020; Singh et al., 2018) Therefore, tracking land use and land-cover change (LULCC) is essential to support policymakers in developing sustainable spatial plans.

Over the last few decades, researchers have used different approaches to classify LULC. For example, (Goodin et al., 2015) used an object-based classification approach in complex agricultural areas along the border between Ukraine and Poland by utilising Landsat 8 OLI data. Another study (Mohajane et al., 2018) used a supervised maximum likelihood to estimate changes in vegetation cover in Azrou Forest, Morocco, using the Landsat data series (1987–2017). Furthermore, Van Leeuwen et al. (2020) compared three machine learning algorithms (random forest, artificial neural network, and support vector machine) for classifying LULC in a temporarily inundated area of Hungary.

The development of geospatial analysis technology currently leads to cloud computing, which can help researchers who lack the IT resources to process their data in the cloud. Google Earth Engine (GEE) is a cloud-based earth observation (EO) platform. GEE allows users to access high-performance computing resources, a multi-petabyte catalogue of satellite imagery, and scientific datasets such as climate, weather, and elevation/terrain (Gorelick et al., 2017). GEE also provides a variety of machine learning classifier algorithms, including CART (classification and regression trees), random forest, SVM (support vector machine), and Naïve Bayes. For example, (Lin et al., 2020) used GEE to monitor LULCC (sandy land, built-up land, cultivated land, forest land, other lands, and water) on the rapidly urbanising island of Haitan, China. Previously, (Zurqani et al., 2018) utilised GEE to analyse four LULCC periods (1999, 2005, 2009, 2015) in the Savannah River basin in South Carolina and Georgia, US. Both studies (Zurqani et al., 2018) used random forest (RF) to classify their imagery. Furthermore, RF is a commonly used machine learning classifier (other than SVM and CART) that performs well for LULC classification (Breiman, 2001; Camargo et al., 2019; Gislason et al., 2006; Pan et al., 2021).

This study aims to assess and interpret LULC changes occurring in East Java Province, Indonesia. This province is the third most populated region in Indonesia. The rapid population growth occupies more land resources for housing, agricultural fields, public infrastructure, road networks, and industrial facilities. As a consequence, rapid LULC change has occurred. Therefore, the assessment of LULC change is used to support the government, decision-makers, and stakeholders for further planning, monitoring, and evaluation of development programs in East Java.

In brief, Sentinel 2 images have the finest spatial resolution at 10 m and temporal (or revisit period) at five days. Therefore, the collection of Sentinel 2 images is more abundant for global mapping. This collection offers more comprehensive and complete data for mapping in every location worldwide (Tong et al., 2020).

In this study, a series of optical images (Sentinel-2) collected from 2015 to 2021 are explored as the primary input for this study. This study also aims to implement GEE by using and exploring an RF classifier.

The classification process is performed on GEE using the Random Forest (RF) classifier. The RF classifier consists of many individual decision trees operating as an ensemble, and the results are based on votes for the most popular classes (Breiman, 2001). Many researchers have used the RF classifier because it provides convincing accuracy (Floreano & de Moraes, 2021; Lin et al., 2020; Pelletier et al., 2016; Tassi & Vizzari, 2020; Tian et al., 2016; Zurqani et al., 2018).

2. Study area

East Java province is the Eastern part of Java Island, Indonesia. The province covers about 38 administrative sub-areas (consisting of municipalities and regencies), covering a total extent of ±47075.35 km^2. East Java is a province known as a national food barn, with Indonesia's largest harvested areas, productivity, and rice production (BPS-Statistics Indonesia, 2021).

This area has a tropical climate with dry and rainy seasons, with an average temperature of 28.2°C and average annual precipitation of 2808.4 mm (BPS-Statistics of Jawa Timur Province, 2021). The elevation (Fig. 1) ranges from ±2 to 3669 meters above sea level (ASL) based on 30 m Digital Elevation Model (DEM) data from the Shuttle Radar Topography Mission (National Aeronautics and Space Administration [NASA] JPL, 2013).

East Java was chosen as the area for this study because this province is unique. For example, the northern part of the province has a relatively dry or arid area composed of limestone mountains (Kendeng Mountains). In the middle area of the region, the more fertile soil occupies an area of alluvial deposits resulting from an active volcano. Furthermore, there are relatively fertile soils within hilly contours in the southern mountain part of the province (Susilohadi, 1995). Moreover, East Java is located right above the Alpine belt, resulting in active volcanoes on its surface. One of the highest volcanoes in Java is Mount Semeru, which experienced a major volcanic eruption in December 2021 (Global Volcanism Program, 2013).

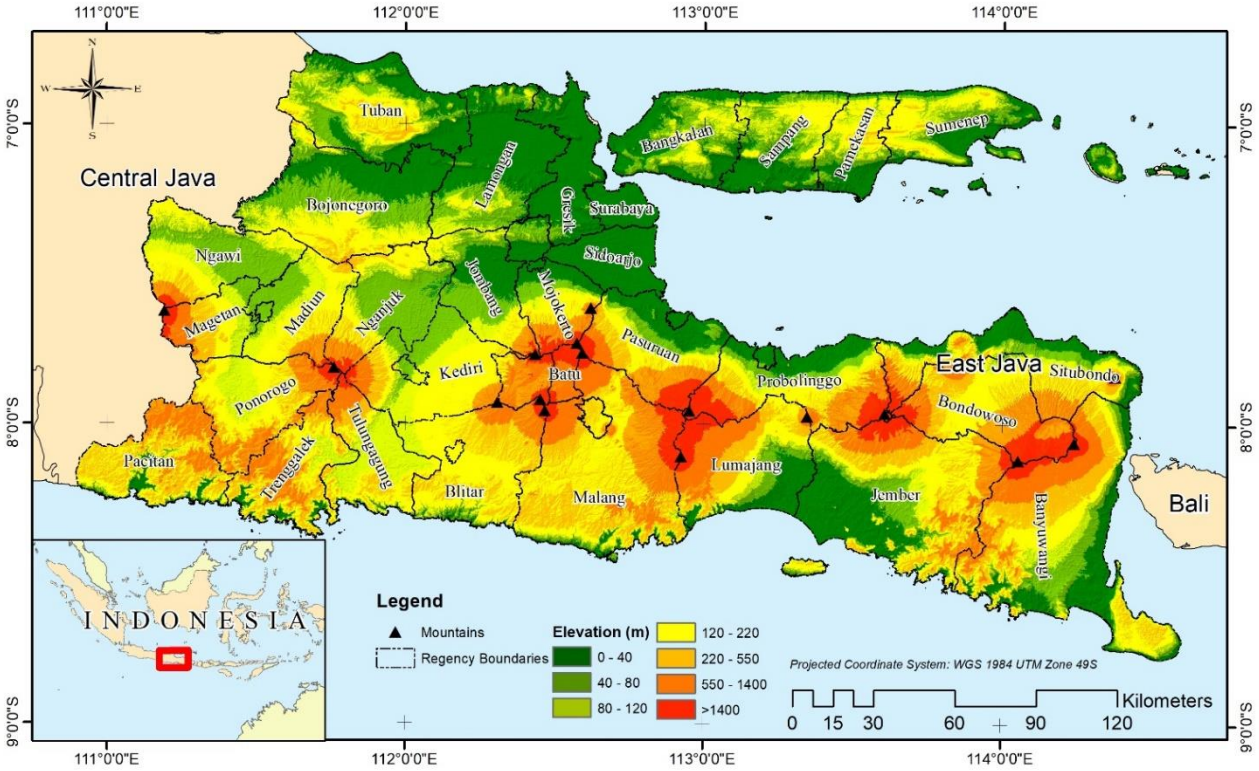

Fig. 1. Study area: East Java Province

3. Materials and methods

Two types of Sentinel-2 products are used as the primary input. A composite image of sentinel 2, known as the top of atmosphere (TOA) product, recorded from 2015 to 2017, represents the first period. However, the Sentinel 2 – TOA product was discontinued after 2017. Then, another type of product, Sentinel 2 – surface reflectance (SR) recorded from 2020 to 2021, was used to represent the second period. The Sentinel 2 – SR product has been freely available on the Earth Engine Data Catalogue since 2017 (GORELICK ET AL., 2017). Therefore, for period 1, the composite uses the TOA product. Thus, this study used data products (TOA and SR) as the primary input.

One challenge in tropical regions is obtaining a series of images free from clouds (INDARTO & HAKIM, 2021). The broader study area (±47075.35 km^2) demands more images to build a composite image free from clouds. Therefore, in this case, a series of images from 2015 to 2017 were collected to produce a single composite image for the first period. Then, a series of images from 2000 to 2001 were assembled to make a single composite representing the second period. Moreover, 740 scenes were collected to build one single composite file by the aggregation method to describe period 1, and 781 scenes were mosaicked to produce a single composite image representing period 2. The aggregation used the median value for each pixel from all images.

Figure 2 shows the general data processing procedures used in this study. Firstly (filtering and cloud mask), the processing procedure in the GEE Code Editor was performed by compiling two customised scripts for each period. The script consisted of five main processes, which included:

1. cloud-free TOA & SR Sentinel 2 image collection;
2. image clipping and training samples collection;
3. classification process using Random Forest;
4. accuracy assessment; and
5. export classified images.

Then, four customised filters were used during the image selection to limit the acquired images, i.e., period of interest (2015–2017 and 2020–2021), cloud cover percentage (10), boundary (East Java), and cloud mask (maskS2clouds). The cloud mask enabled cloudy and cloud-free pixels to be distinguished. The mask included dense and cirrus clouds with an indicator specifying the cloud type (SENTINEL 2 PDGS PROJECT TEAM, 2014). The filtering produced two image collections by using computed median bands. Both composite images (periods 1 and 2) used the red, green, blue (RGB), near-infrared (NIR), red-edge, and short-wave infrared bands.

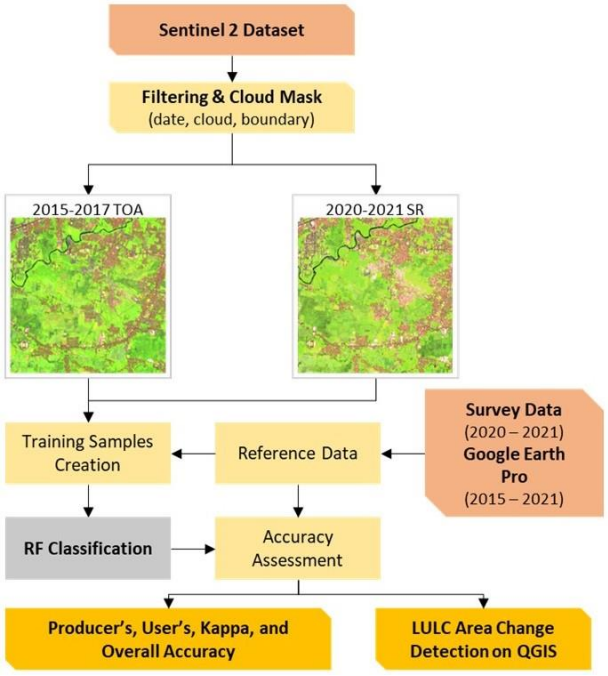

Fig. 2. Flowchart showing the procedures for data processing

Secondly (training samples creation), a field survey was conducted to collect reference LULC features (Ground control point or GCP) at different locations using an RGB Camera, UAV, and hand-held GPS. In this study, for areas that were difficult to access, such as mountain craters, dense forests, and remote regions, GCPs were obtained by observing the Google Earth Images for the second period (2020–2021). Furthermore, GCPa was also derived by observing Google Earth images from historical images to represent the features for period 1 (2015 to 2017).

Thirdly (RF Classification), for each period (periods 1 & 2), at least 500 GCPs were included in data processing, which was divided into 70% point (GCPs) utilised for training samples and 30% of GCPs used for accuracy assessment. In this study, the primary land cover features were represented by eight classes, as shown in Table 1. The classification was based on the terminology published in the National standard map (BIG, 2018), a field survey, and the interpretation of Sentinel 2 composites of each period.

Table 1. Description of LULC classes

Classes	Code	Description
Built-up area	BU	All artificial surface features observed in the study area, i.e., settlements, buildings, roads, concrete, etc., were built to support human activities.
Heterogeneous Agricultural Land	HAL	It included all agricultural areas other than paddy fields, such as dryland farming or seasonal crops, i.e., corn, sugarcane, soybean, and cassava.
Bare Soil	BS	The barren surface is covered by sand or rock with little or no vegetation. The sand was most typically seen along coastlines. Most of the rock was found in mining and mountain/hill locations.
Paddy field	PF	Agricultural land specifically for paddy fields
Open water	OW	Land features submerged under deep water, such as lakes, rivers, and reservoirs.
Vegetation	VG	All non-agricultural plants, including woody perennial plants, dense tropical forests, mixed forests, and plantations.
Shrubland	SH	All surface features, including grass, bush, arid landscapes with sparse/less vegetation, and vacant farmland.
Wetland	WL	Surface features dominated by shallow water, inundated areas, or ponds. Wetlands are commonly found around seashores. These landmarks are present in the northern section of the main island of East Java.

Fourthly, the accuracy assessment of the classification processes was calculated by a confusion matrix to determine the kappa, overall, producer, and user accuracy (STORY & CONGALTON, 1986; Kappa accuracy (kappa index) was defined as follows:

$$k = \frac{Observed - Expected}{1 - Expected} \qquad \text{equation (1)}$$

"Observed" means the overall value for "percentage correct" obtained from dividing the sum of diagonal entries by the sum of the total sample. While "Expected" is an estimate of the contribution of a chance agreement to the observed percentage correct. "Expected" represents a prediction of the likelihood of chance agreement influencing the observed ratio of correctness. The calculation of "expected" values involves using the totals of rows and columns (referred to as "marginals"). The multiplication of these row and column marginals helps estimate the pixel counts assigned to each cell in the confusion matrix,

assuming pixels are randomly assigned to each category (CAMPBELL, 2008). Producer's accuracy (PA) is the ratio of correctly classified pixels to the total pixels of that class in the error matrix. It gauges how well reference pixels are classified, including the error of omission. User's accuracy (UA) is the ratio of correctly classified pixels to the total pixels classified. UA measures the map's reliability, indicating how accurately it represents the ground conditions (PATEL & KAUSHAL, 2010). Utilisation of these indices (overall, kappa, producers, and user accuracy) is a standard method used to measure the correctness of image classification (CAMPBELL & WYNNE, 2011; VADREVU, 2013; AMINI ET AL., 2022; FOODY, 2020; KHOSHNOOD MOTLAGH ET AL., 2021; POVEDA-SOTELO ET AL., 2022).

4. Results and discussion

4.1. Accuracy assessment

The accuracy assessment (Table 2) shows a good result on both maps. The overall accuracy values obtained were 92.64% (Period 1) and 92.27% (Period 2). Meanwhile, the Kappa accuracy values obtained were 91.09% (Period 1) and 90.70% (Period 2). Producer and user accuracy values ranged from 81% to 100%. The lowest accuracy assessment value was in SH, and the highest was in OW. SH shows low accuracy because, in the field, SH is mixed with other classes, making it harder to distinguish.

Table 2. LULC accuracy assessment results

Assessment	Period	Classes								OA	KA
		BU	HAL	BS	PF	OW	VG	SH	WL		
UA (%)	1	92.93	91.78	100.00	90.60	100.00	94.49	85.33	91.18	92.64	91.09
PA (%)		91.54	92.63	91.46	92.58	100.00	95.71	82.05	100.00		
UA (%)	2	91.96	92.92	89.38	92.61	92.59	96.67	84.69	100.00	92.27	90.70
PA (%)		87.56	91.30	100.00	92.97	100.00	100.00	81.37	93.75		

Note: UA (User's Accuracy), PA (Producer's Accuracy), OA (Overall Accuracy), KA (Kappa Accuracy)

4.2. Classification results

Figure 3 shows the LULC classification results for both periods. The classification produced eight major LULC classes, i.e., built-up area (BU), heterogeneous-agricultural land (HAL), bare soil (BS), paddy field (PF), open water (OW), vegetation (VG), shrubland (SH), and wetland (WL). Each of the three main classes (PF, VG, SH) occupied more than 10% of the space in East Java (Table 2). The most extensive areas were occupied by paddy fields (PF). PF occupied more than 40% of the total. Then, VG (vegetation) covered more than 30% of the total area.

4.3. LULC Change (gains and losses)

Table 3 summarises the LULC Change from 2015 to 2021. Significant Change (more than 10%) occurred for PF and VG.

The Paddy field (PF) was the most extensive area for the two periods (Table 3). In Period 1, the PF covered 18981.66 km^2 (40.32%), and in Period 2, it covered 21707.83 (46.11%), an increase of +14.36% over six years (from 2015 to 2021).

Figure 4 shows the loss and gain analysis for the LULC Change from 2015 to 2021. Four classes experienced an increase in area, i.e., BU (30.23%), HAL (30.77%), BS (24.52%), and PF (14.36%). As a consequence, the other four classes decreased, i.e., OW (-32.79%), VG (-25.72%), SH (-6.59%), and WL (-25.53%).

Population increase seems to be one of the causes of BU land expansion. Since 2015, the population in the study area increased by 4.87%, from 38.78 to 40.67 million people (BPS-STATISTICS OF JAWA TIMUR PROVINCE, 2021). BU increased quite a lot due to the conversion from PF (569 km^2), HAL (326 km^2), SH (133 km^2), and BS (134 km^2).

HAL has expanded by 885.40 km^2 over a year. One of the reasons for this expansion is the increasing need for food crops besides rice, vegetables, and fruit. The gain was transferred from PF (601 km^2) and SH (534 km^2). Meanwhile, the BS experienced a minor increase (177.96 km^2). The gain was obtained from VG (81 km^2), PF (141 km^2), which was not in its growing season, HAL, SH, and the drying up of WL.

SH experienced quite a lot of conversion. The analysis showed a total loss of 4529.09 km^2 and a total gain of 4124.96 km^2. The loss was due to the conversion of SH into HAL (1160 km^2), PF (1819 km^2), and VG

(1261 km^2). Meanwhile, the gain was significant due to the conversion from PF (2626 km^2) and VG (817 km^2). During the last six years, PF and VG have changed significantly. The calculation results show that there has been a reasonably large land conversion from VG covering an area of 5073 km^2 into PF and 817 km^2 into SH (Table 4). PF gain area was also quite substantial from the conversion of SH covering an area of 1819 km^2. The loss and gain visualisation of vegetation and PF are shown in Figure 5.

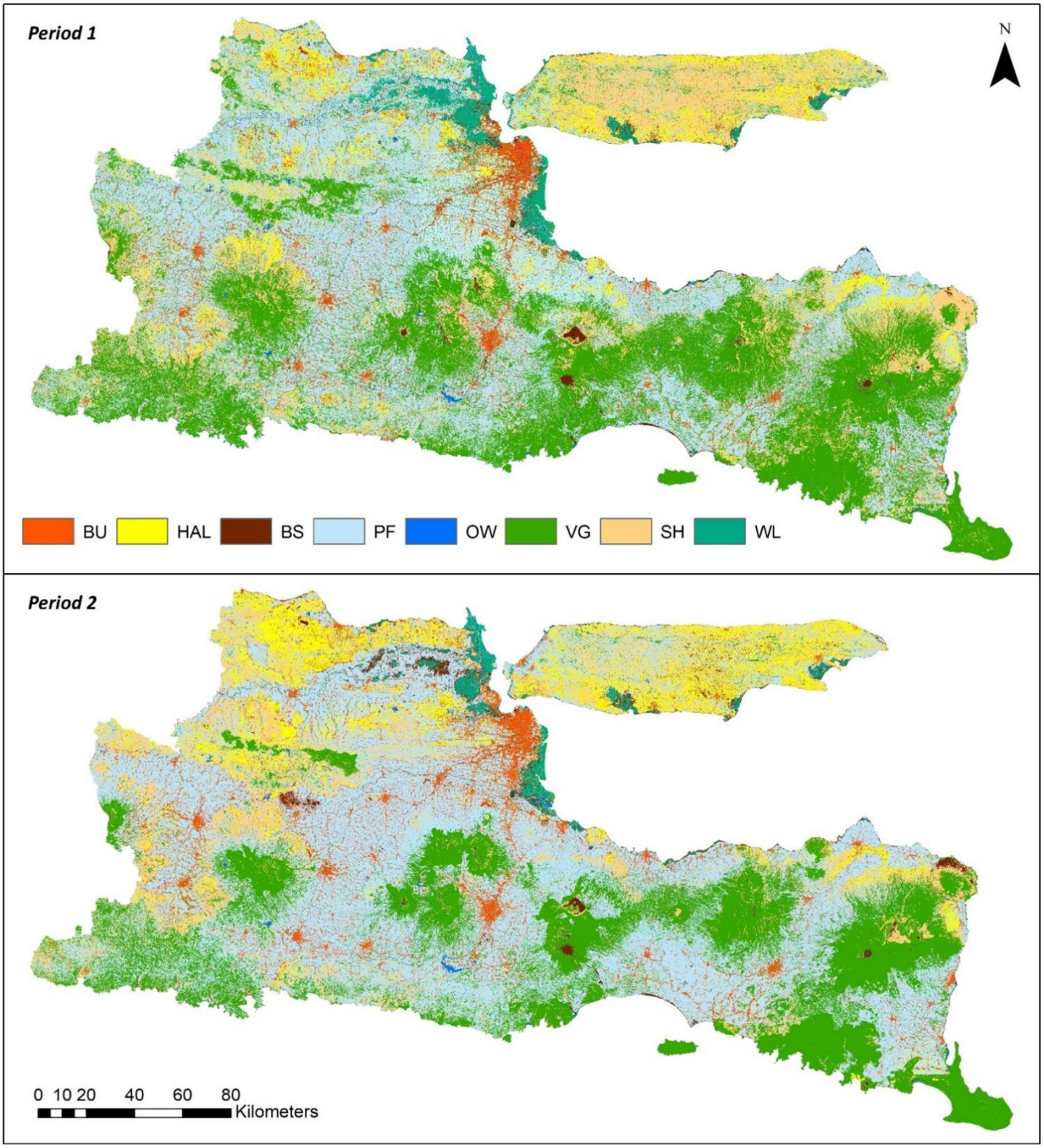

Fig. 3. LULC classification of East Java, Note: BU (Built-up land), HAL (Hetero-Agri Land), BS (Bare Soil), PF (Paddy Field), OW (Open Water), VG (Vegetation), SH (Shrub), WL (Wetland)

Table 3. LULC area of each class

LULC Types	Period 1		Period 2	
	km^2	%	km^2	%
Built up area (BU)	2403.84	5.11	3130.44	6.65
Heterogeneous Agricultural Land (HAL)	2877.62	6.11	3763.01	7.99
Bare Soil (BS)	725.66	1.54	903.62	1.92
Paddy Field (PF)	18981.66	40.32	21707.83	46.11
Open Water (OW)	144.29	0.31	96.98	0.21
Vegetation (VG)	14930.11	31.72	11090.26	23.56
Shrubland (SH)	6130.84	13.02	5726.90	12.17
Wetland (WL)	881.33	1.87	656.30	1.39
Total	47075.35	100.00	47075.35	100.00

Fig. 4. LULC net change

Table 4. LULC transition matrix (km^2)

	BU	HAL	BS	PF	OW	VG	SH	WL	Total
BU	1870	161	35	218	0	7	112	2	2404
HAL	326	1366	31	601	0	19	534	0	2878
BS	134	46	261	141	7	81	29	26	726
PF	569	925	191	13734	2	921	2626	14	18982
OW	1	0	16	12	62	6	1	48	144
VG	96	106	51	5073	3	8777	817	7	14930
SH	133	1160	155	1819	0	1261	1602	0	6131
WL	5	0	175	107	24	6	6	557	881
Total	3134	3765	914	21704	98	11078	5727	654	47075

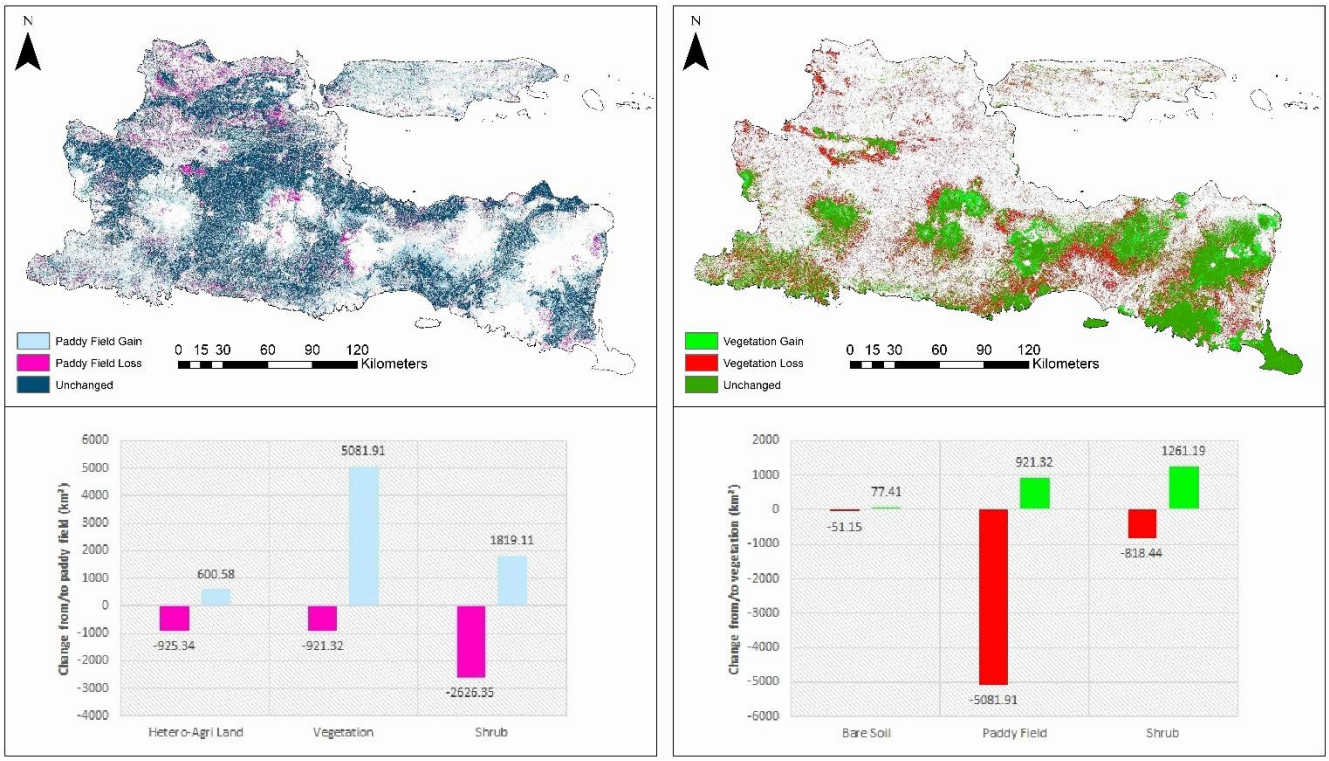

Fig. 5. Vegetation and paddy field loss and gains

4.4. LULC change in the urbanised areas

The Surabaya Metropolitan, which includes Surabaya, Gresik, Sidoarjo, and Mojokerto cities, has occupied the most urbanised areas in the province. The 2020 survey data from the Statistical Agency (BPS-Statistics of Jawa Timur Province, 2023) collected about 2,934 large and medium industries in this region, representing approximately 50.4% of all large and medium enterprises. The percentage (50,4%) increased by 4.52% from 2015 (only 2807 industries). The survey results (BPS-Statistics of Jawa Timur Province, 2023) also showed that in 2020, more than 4.4×10^5 workers were employed in these industries. Population survey results showed an increase of 2.46% from 2015 to 2021 in Surabaya Metropolitan. In addition, approximately 68593 micro and small industries included more than 1.6×10^5 workers with many sectors and a high minimum wage based on The East Java Governor's Decree (2020), which encouraged many people in other areas to look for work and settle there.

The results for Surabaya Metropolitan (Figs 6 and 7) show an expanded built-up area of 109.61 km^2 (+22.24%). The results of field surveys and observations through Google Earth (Fig. 8) show that the construction of new settlements is one form of this expansion. The formation of this new settlement cannot be separated from the increasing number of existing residents and additional newcomers from other cities working in this area. Consequently, PF and WL experienced a decrease in the area because of conversion into BU by 34.61 and 67.27 km^2, respectively.

The cloud-free image collection for 2020–2021 shows that the region was in the dry season. Meanwhile, the cloud-free image collection for the 2015–2017 period shows that the area was in the wet season. Thus, as a consequence, VG, PF, OW, and WL all decreased. Meanwhile, HAL, BS, and SH increased due to the drying areas.

4.5. LULC change in agricultural regions

Jember Regency is a relatively fertile area suitable for developing agricultural and plantation commodities in East Java. Most of this region's land is 0–100 meters above sea level. The average annual rainfall (1999–2020) is 1622.99 mm. Most agricultural and plantation commodities are widely produced in this region, including rice, corn, soybeans, sugar cane, chilli, oranges, coconut, coffee, cocoa, and tobacco (BPS-Statistics of Jember Regency, 2021) (Fig. 9).

Fig. 6. LULC net change in Surabaya Metropolitan

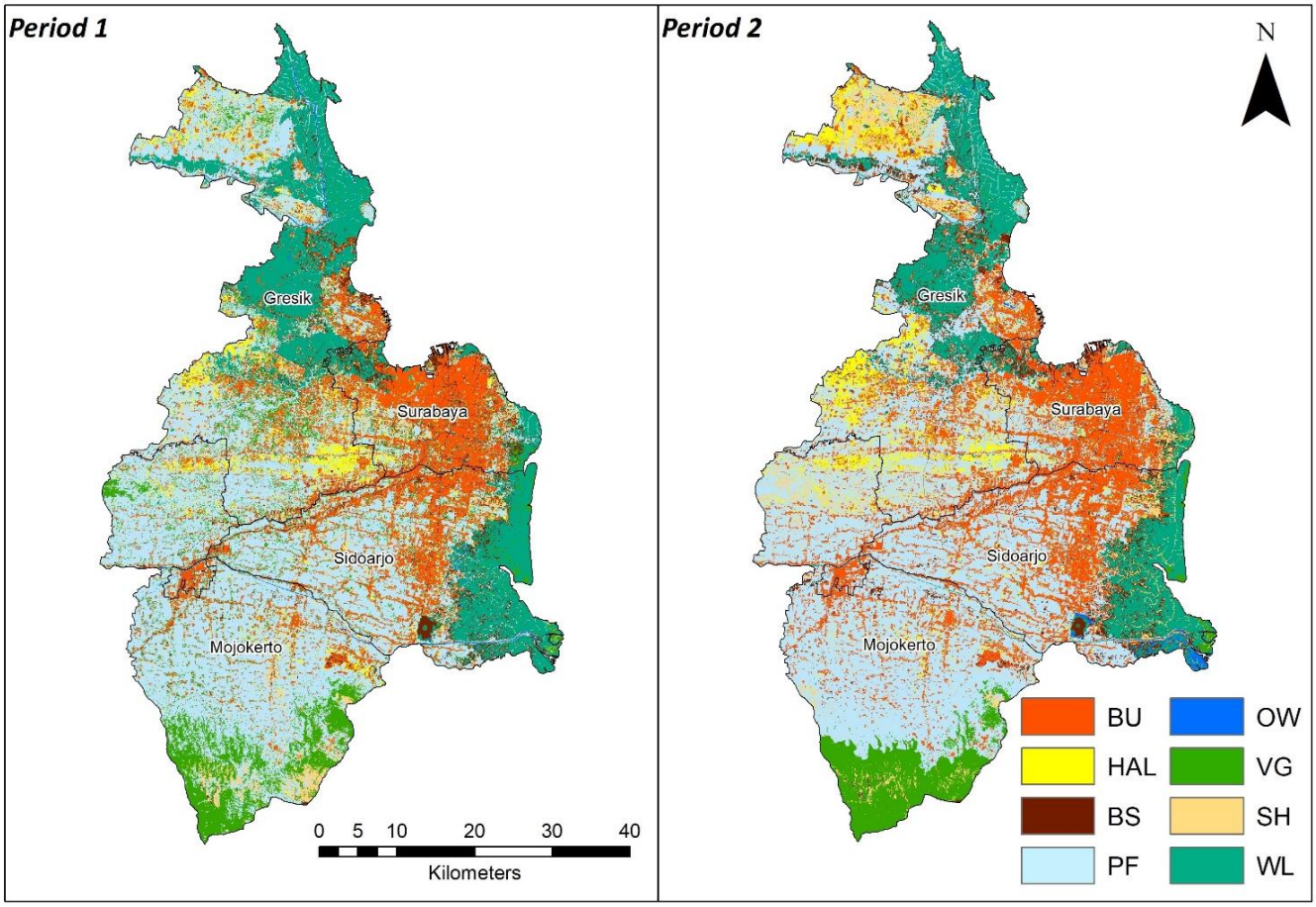

Fig. 7. LULC maps show the rapid development of urban areas from period 1 to period 2

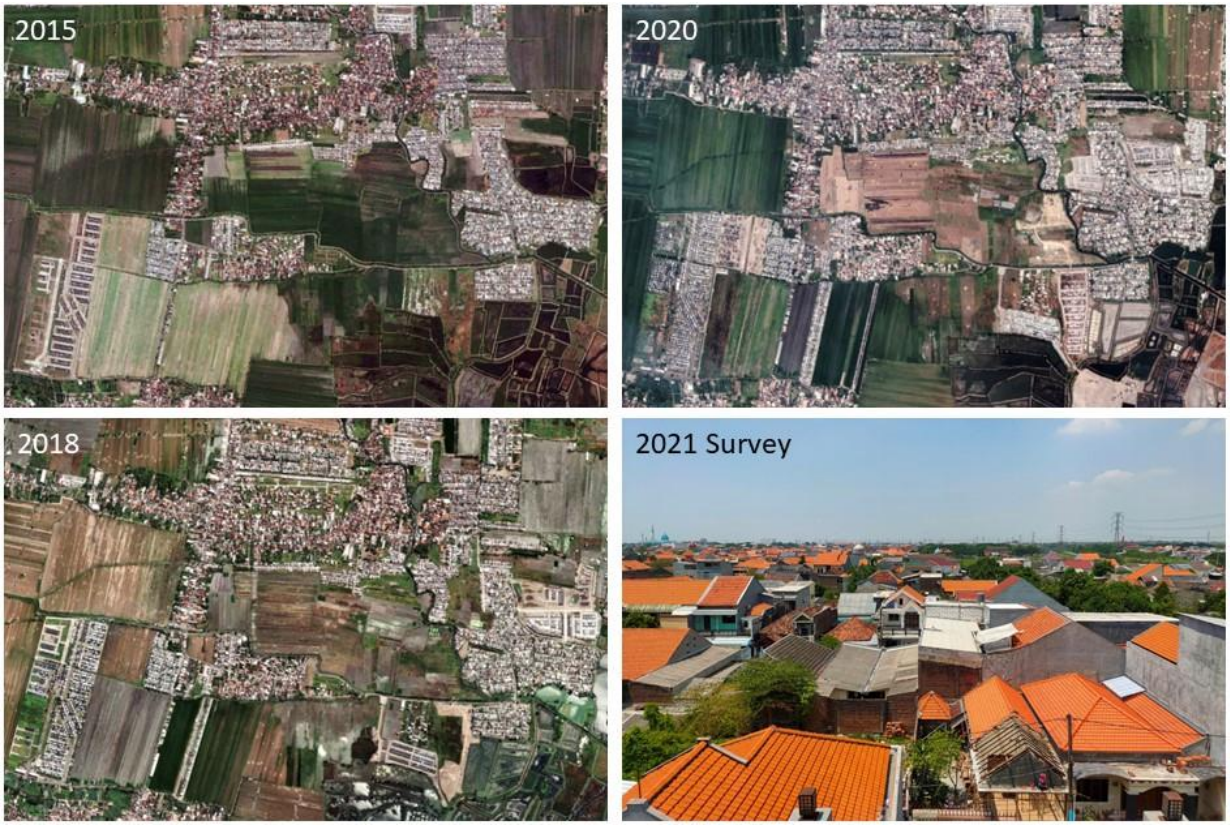

Fig. 8. Gains in built-up area from 2015 to 2020

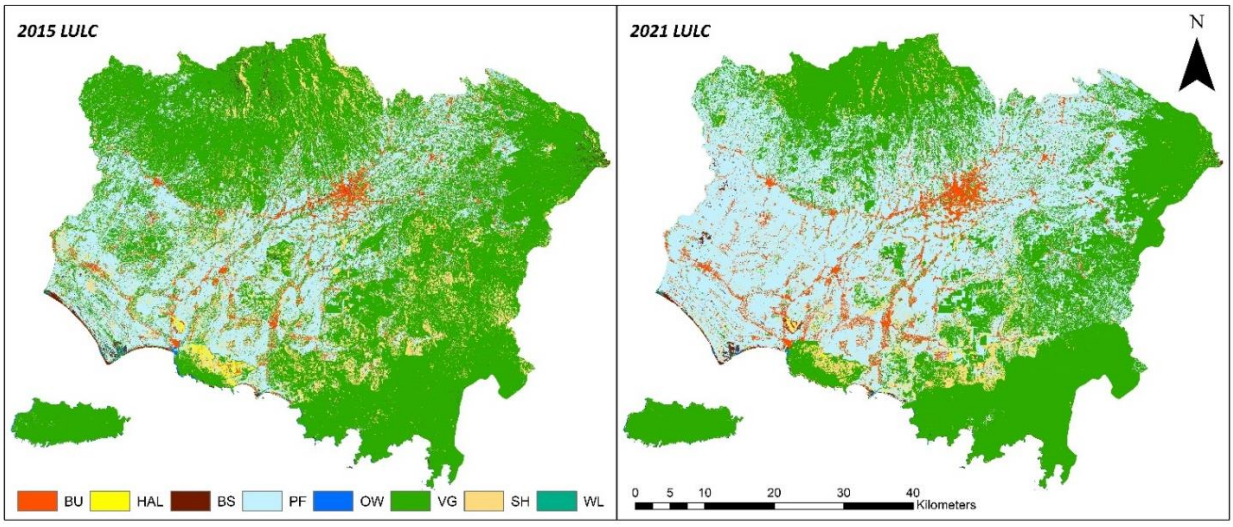

Fig. 9. LULC maps of Jember Regency

The results (Table 5) show a massive expansion of BU in this area, from 107.06 to 168.57 km^2 (+57.45%). PF also experienced very significant increases. In 2015, the measured PF area was 870.95 km^2 and increased to 1495.02 km^2 (+71.65%) in 2021. The observation results through Google Earth, shown in Figure 10, indicate new agricultural land clearings. These land clearings mainly occurred in the foothills, previously a VG area. In addition, another cause of expansion was due to other LULC classes, such as HAL and VG, being misclassified into PF. This misclassification occurred because HAL and VG are mixed with the PF in the field, making it difficult to separate.

A decrease in other LULC class areas is due to the expansion of BU and PF. Furthermore, the paddy was planted when the images were acquired and propagated the decline in HAL classes.

Table 5. LULC change of Jember Regency

	2015		2021		Net Change	
	km²	%	km²	%	km²	pp
BU	107.06	3.23	168.57	5.09	61.51	1.86
HAL	28.81	0.87	12.90	0.39	-15.91	-0.48
BS	27.42	0.83	18.87	0.57	-8.55	-0.26
PF	870.95	26.29	1495.02	45.14	624.07	18.84
OW	6.36	0.19	3.22	0.10	-3.14	-0.09
VG	1982.80	59.86	1447.43	43.70	-533.36	-16.16
SH	283.83	8.57	163.27	4.93	-120.57	-3.64
WL	5.08	0.15	3.04	0.09	-2.05	-0.06
Total	3312.32	100.00	3312.32	100.00		

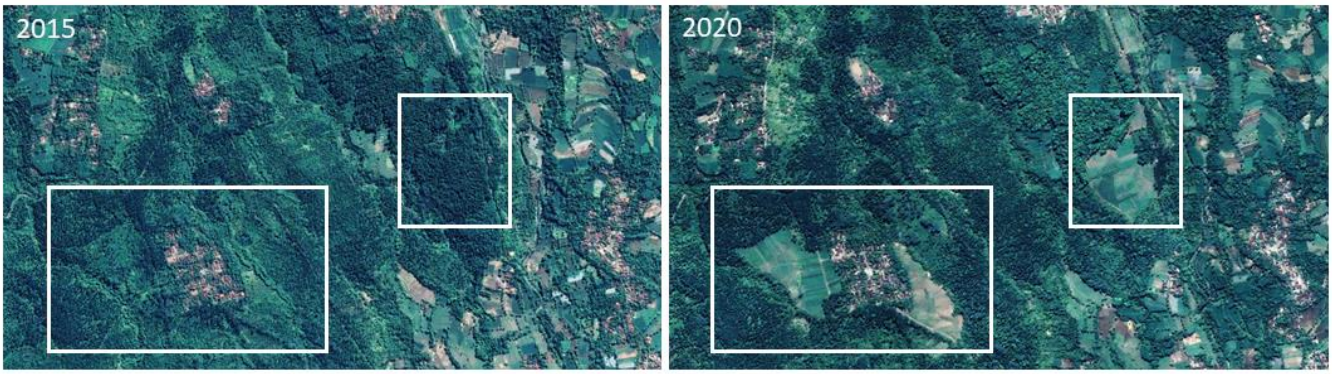

Fig. 10. New agricultural land clearings from 2015 to 2020

5. Conclusion

The two classified maps show promising accuracy results. The overall accuracy values obtained were 92.64% in 2015 and 92.27% in 2021. Meanwhile, the Kappa accuracy values obtained were 91.09% in 2015 and 90.70% in 2021. Moreover, producer and user accuracy values range from 81% to 100%. The result shows that significant LULC Change is more marked in the most urbanised areas (in and around the big cities), followed by LULC change in and around medium towns and rural areas. Four classes experienced an area increase, i.e., BU (+30.23%), HAL (+30.77%), BS (+24.52%), and PF (+14.36%). As a consequence, the other four classes compensate for the increase, i.e., OW (-32.79%), VG (-25.72%), SH (-6.59%), and WL (-25.53%). In conclusion, using optical imagery from Sentinel 2 processed by GEE shows its capability to track, classify, and interpret the main LULC change of east Java province from 2015 to 2021.

Acknowledgement

This work was supported by DRTPM-Kemendikbudristek 2023 using skim Penelitian Dasar Kerjasama Dalam Negri led by Marga Mandala (SK no: 0557/E5.5/AL.04/2023).

References

Aksoy H., Kaptan S. 2020. Simulation of future forest and land use/cover changes (2019–2039) using the cellular automata-Markov model. *Geocarto International*, *6049*.

Amini S., Saber M., Rabiei-Dastjerdi H., Homayouni S. 2022. Urban Land Use and Land Cover Change Analysis Using Random Forest Classification of Landsat Time Series. *Remote Sensing*, 14(11), 2654.

BIG. 2018. *Peta Rupa Bumi Indonesia Skala 1:25.000*.

BPS-Statistics Indonesia. 2021. *Luas Panen, Produksi, dan Produktivitas Padi Menurut Provinsi 2019-2021 [Harvested Area, Production, and Productivity of Paddy Based on Province 2019-2021]*. BPS-Statistics Indonesia.

BPS-Statistics of Jawa Timur Province. 2021. *Provinsi Jawa Timur dalam Angka 2021 [Jawa Timur Province in Figures 2021]*. BPS-Statistics of Jawa Timur Province.

BPS-Statistics of Jawa Timur Province. 2023. *Provinsi Jawa Timur dalam Angka 2023 [Jawa Timur Province in Figures 2023]*. BPS-Statistics of Jawa Timur Province.

BPS-Statistics of Jember Regency. 2021. *Kabupaten Jember dalam Angka 2021 [Jember Regency in Figures 2021]*. BPS-Statistics of Jember Regency.

Breiman L. 2001. Random Forests. *Machine Learning*, 45(1): 5–32.

Camargo F.F., Sano E.E., Almeida C.M., Mura J.C., Almeida T. 2019. A comparative assessment of machine-learning techniques for land use and land cover classification of the Brazilian tropical savanna using ALOS-2/PALSAR-2 polarimetric images. *Remote Sensing*, 11(13), 1600.

Campbell J.B. 2008. *Introduction to Remote Sensing, 4th ed.* (4th ed.). The Guilford Press.

Campbell J.B., Wynne R H. 2011. *Introduction to Remote Sensing, Fifth Edition*. Guilford

East Java Governor's Decree. 2020. *Keputusan Gubernur Jawa Timur Nomor 188/538/KPTS/013/2020 Tentang Upah Minimum Kabupaten/Kota di Jawa Timur Tahun 2021 [East Java Governor's Decree Number 177/538/KPTS/013/2020 About Minimum Wages of Municipality/Regency in East Java Province]*.

Fonji S.F., Taff G.N. 2014. Using satellite data to monitor land-use land-cover change in northeastern Latvia. *SpringerPlus*, 3(1), 61.

Foody G.M. 2020. Explaining the unsuitability of the kappa coefficient in the assessment and comparison of the accuracy of thematic maps obtained by image classification. *Remote Sensing of Environment*, 239, 111630.

Gashu K., Gebre-Egziabher T. 2018. Spatio-temporal trends of urban land use/land cover and green infrastructure change in Bahir Dar and Hawassa in two Ethiopian cities. *Environmental Systems Research*, 7(8).

Gislason P.O., Benediktsson J.A., Sveinsson J.R. 2006. Random forests for land cover classification. *Pattern Recognition Letters*, 27(4): 294–300.

Global Volcanism Program. 2013. Semeru (263300) in Volcanoes of the World. *Smithsonian Institution*, v.4.10.6.

Goodin D.G., Anibas K.L., Bezymennyi M. 2015. Mapping land cover and land use from object-based classification: an example from a complex agricultural landscape. *International Journal of Remote Sensing*, 36(18): 4702–4723.

Gorelick N., Hancher M., Dixon M., Ilyushchenko S., Thau D., Moore R. 2017. Google Earth Engine: Planetary-scale geospatial analysis for everyone. *Remote Sensing of Environment*, 202: 18–27.

Hariyono M. I. (n.d.). *Kajian Perubahan Penutup Lahan Peta Rupabumi pada Skala yang Berbeda*.

Hassan Z., Shabbir R., Ahmad S. S., Malik A. H., Aziz N., Butt A., Erum S. 2016. Dynamics of land use and land cover change (LULCC) using geospatial techniques: a case study of Islamabad Pakistan. *SpringerPlus*, 5(1).

Hu Y., Batunacun Zhen L., Zhuang D. 2019. Assessment of Land-Use and Land-Cover Change in Guangxi, China. *Scientific Reports*, *9*(1): 1–13.

Khoshnood Motlagh S., Sadoddin A., Haghnegahdar A., Razavi S., Salmanmahiny A., Ghorbani K. 2021. Analysis and prediction of land cover changes using the land change modeller (LCM) in a semiarid river basin in Iran. *Land Degradation and Development*, 32(10): 3092–3105.

Lin L., Hao Z., Post C.J., Mikhailova E.A., Yu K., Yang L., Liu J. 2020. Monitoring land cover change on a rapidly urbanising island using Google Earth engine. *Applied Sciences (Switzerland)*, 10(20), 1–16.

Lin S.-K. 2013. *Introduction to Remote Sensing*. 5th Edition. Campbell J.B. & Wynne R.H. (eds). *Remote Sensing*, 5, 1: 282–283.

Mohajane M., Essahlaoui A., Oudija F., Hafyani M. El Hmaidi A. El OualiA. El Randazzo G., Teodoro A. C. 2018. Land use/land cover (LULC) using Landsat data series (MSS, TM, ETM+, and OLI) in Azrou forest in the central middle atlas of Morocco. *Environments - MDPI*, 5(12): 1–16.

National Aeronautics and Space Administration [NASA] JPL. 2013. *NASA Shuttle Radar Topography Mission Global 1 arc second [Data set]*. NASA EOSDIS Land Processes DAAC.

Pan X., Wang Z., Gao Y., Dang X., Han Y. 2021. Detailed and automated land use/land cover classification using machine learning algorithms in Google Earth Engine. *Geocarto International*, 0(0): 1–18.

Patel N., Kaushal B.K. 2010. Improvement of User's Accuracy through Classification of Principal Component Images and Stacked Temporal Images. *Geospatial Information Science*, *13*(4), 243–248.

Poveda-Sotelo Y., Bermúdez-Cella M.A., Gil-Leguizamón P. 2022. Evaluation of supervised classification methods for estimating spatiotemporal changes in the Merchán and Telecom paramos, Colombia. *Boletin de Geologia*, 44(2): 51–72.

Sentinel 2 PDGS Project Team. 2014. *Sentinel-2 Calibration and Validation Plan for the Operational Phase Bianca Hoersch* (Issue 1). ESA Centre for Earth Observation.

Shih H. Chien Stow D.A., Chang K.C., Roberts D.A., Goulias K.G. 2021. From land cover to land use: Applying random forest classifier to Landsat imagery for urban land-use change mapping. *Geocarto International*, 0(0): 1–24.

Singh S.K., Laari P.B., Mustak S., Srivastava P.K., Szabó S. 2018. Modeling land use land cover change using earth observation datasets of Tons River Basin, Madhya Pradesh, India. *Geocarto International*, 33(11): 1202–1222.

Story M., Congalton R.G. 1986. Remote Sensing Brief Accuracy Assessment: A User's Perspective. *Photogrammetric Engineering and Remote Sensing*, 52(3): 397–399.

Susilohadi. 1995. *Late tertiary and quaternary geology of the East Java Basin, Indonesia [Doctor of Philosophy thesis]*. University of Wollongong.

Zurqani H.A., Post C.J., Mikhailova E.A., Schlautman M.A., Sharp J.L. 2018. Geospatial analysis of land use change in the Savannah River Basin using Google Earth Engine. *International Journal of Applied Earth Observation and Geoinformation*, 69: 175–185.